05905

LA-UR- 09-05705

Approved for public release;
distribution is unlimited.

Title:	Shock Wave Structure for a Fully Ionized Plasma
Author(s):	Thomas O. Masser (CCS-2) John G. Wohlbier (CCS-2) Robert B. Lowrie (CCS-2)
Intended for:	Shock Waves

Los Alamos
NATIONAL LABORATORY
EST. 1943

Form 836 (7/06)

Los Alamos
NATIONAL LABORATORY
research note
Weapons Supported Research
Radiation Hydrodynamics

To/MS: Distribution
From/MS: Robert B. Lowrie/CCS-2, MS D413
John G. Wohlbier/CCS-2, MS D413
Thomas O. Masser/CCS-2, MS K784
Phone/FAX: (505)667–2121
Symbol: LA-UR-07-xxxx
Date: September 3, 2009

Subject: Shock Wave Structure for Fully Ionized Plasma

Executive Summary

We study the structure of planar shock waves in a two-temperature model of a fully ionized plasma that includes electron heat conduction and energy exchange between electrons and ions. For steady flow in a reference frame moving with the shock, the model reduces to an autonomous system of ordinary differential equations which can be numerically integrated. A phase space analysis of the ODEs provides additional insight into the structure of the solutions. For example, below a threshold mach number the model produces fully dispersed shocks; while above another threshold mach number, the solutions contain embedded hydrodynamic shocks. Between these two threshold values, the appearance of embedded shocks depends on the electron diffusivity and the electron–ion coupling term. We also find that the ion temperature may continue to increase after the shock and reaches a maximum near the isothermal sonic point. We summarize the methodology for solving for two-temperature shocks, and show results for several values of shock strength and material parameters to quantify the shock structure and explore the range of possible solutions. Such solutions may be used to verify hydrodynamic codes that use similar plasma physics models.

1 Introduction

We study the structure of planar shock waves in a two-temperature model of a fully ionized plasma that includes electron heat conduction and energy exchange between electrons and ions. For steady flow in a reference frame moving with the shock, the model reduces to an autonomous system of ordinary differential equations which can be numerically integrated. The primary focus of this study is to compute and explore the range of possible shock solutions for a model plasma. These solutions may be used to verify hydrodynamic codes that use similar plasma physics models.

The first qualitative picture of the shock wave structure in a two temperature electrically neutral plasma was provided by Zel'dovich, for the case of strong shock waves in air [5]. Shafranov computed the shock profiles for a specific model of hydrogen with shocks of varying strength [4]. Imshennik analyzed a generalized version of Shafranov's model to determine a critical shock strength between fully continuous (fully dispersed) shock profiles and discontinuous (embedded hydrodynamic shocks) shock profiles [2]. Most subsequent work focused on the radiative effects of strong shocks or magnetic field effects in non-neutral plasmas. However, the importance of electron heat conduction in ICF pellets and some astrophysical regimes has made the inclusion of plasma models with separate ion and electron temperatures in simulation codes desirable. Producing analytic (or semi-analytic) solutions for two temperature plasmas in the absence of radiation is useful for the verification of the physics algorithms (or a subset of the physics algorithms) within a full simulation code.

In this study we focus only on the interactions of the electrons and ions with a shock moving through a fully ionized gas. We assume that strong Coulomb interactions keep the electrons and ions rigidly coupled, so that the plasma remains electrically neutral. We neglect all radiative effects and assume that both the electron heat conduction and the energy exchange between the electrons and ions is linear. While the our model will be invalid for determining the true details of plasma shock structures, the solutions described

in this study are simple to compute and provide additional insight into the shock structure. Simulating shocks in plasmas remains a challenging problem and simulation codes should be verified against available exact results [1]. The simple model we employ captures the primary effects of shocks on the electron and ion temperatures and may lead to a more complete picture of the range of possible solutions. For instance, we show that the ion temperature may continue to increase behind a hydrodynamic shock and achieve a maximum in the region downstream of the shock, similar to an effect seen in radiative shocks [3]. We also improve on Imshennik's derivation [2] of the boundary between continuous and discontinuous shock profiles.

In Section (2), we provide the governing equations for and describe our plasma model. In Sections (3-4), we reduce the governing equations to the simple case of a steady shock in a reference frame that is stationary with respect to the shock and describe the overall jump conditions from the upstream to the downstream states and the jump conditions at a shock. In Section (5), we further reduce the governing equations to a 2×2 system of coupled nonlinear ordinary differential equations. In Section (6), we describe the numerical procedure we employ to compute solutions. In Section (7), we depict solutions for several values of material parameters and shock strength and describe two novel observations. We summarize our results and address possible future investigations in Section (8).

2 Governing Equations

Assume a fully-ionized flow of a single material in a 1-D planar geometry. The governing equations are given by

$$\partial_t \rho + \partial_x(\rho v) = 0, \tag{1a}$$

$$\partial_t(\rho v) + \partial_x\left(\rho v^2 + p\right) = 0, \tag{1b}$$

$$\partial_t(\rho E) + \partial_x\left[v\left(\rho E + p\right)\right] = \partial_x(\kappa_e \partial_x T_e), \tag{1c}$$

$$\partial_t(\rho e_e) + \partial_x(\rho v e_e) + p_e \partial_x v = \gamma_{ei}(T_i - T_e) + \partial_x(\kappa_e \partial_x T_e), \tag{1d}$$

where ρ is the density, v the velocity, p the bulk pressure and $\gamma_{ei}(\rho, T_e)$ the electron-ion coupling coefficient. The subscript-$_e$ corresponds to an electron quantity and the subscript-$_i$ denotes an ion quantity. So for example, e_e is the specific electron energy and T_i is the ion temperature. The total material energy is denoted by $E = e + v^2/2$. Also, $\kappa_e(\rho, T_e)$ is the thermal diffusivity for the electrons.

The material's equation-of-state (EOS) is assumed to be of the form

$$p = p(\rho, T), \qquad e = e(\rho, T). \tag{2}$$

The ion and electron quantites are assumed to be related as

$$p = p_i + p_e, \qquad e = e_i + e_e, \tag{3}$$

with the further assumption that

$$e = C_v T = C_{v,i} T_i + C_{v,e} T_e = e_i + e_e. \tag{4}$$

In this ionized flow model, the quantity T is a mathematically useful average of T_i and T_e. Several calculations are simplified by considering T and T_e, instead of T_i and T_e. Physically, we think of $T(x)$ as an equilibrated temperature, the limit of $T_e(x)$ and $T_i(x)$ as $\gamma_{ei} \to \infty$. The ratios of electron and ion specific heats to the bulk specific heat are written as a fractional quantity with the single parameter Z.

$$\frac{C_{v,i}}{C_v} = \frac{1}{Z+1}, \qquad \frac{C_{v,e}}{C_v} = \frac{Z}{Z+1}. \tag{5}$$

Note also that the electron advection equation (Eq. (1d)) can be expressed as

$$\rho T_e \frac{DS_e}{Dt} = \gamma_{ei}(T_i - T_e) + \partial_x(\kappa_e \partial_x T_e) \tag{6}$$

where S_e is the electron entropy. We use Eq. (6) to derive the additional jump condition required for the system (1).

3 The Shock Problem

In this section we define the shock problem we wish to solve. We select a reference frame where the shock speed is zero and the flow moves in the $+x$ direction. The non-zero shock speed case may be found through a Galilean transformation. The reference state (subscript-$_0$) will refer to the far upstream conditions ($x \to -\infty$), while the subscript-$_1$ refers to far downstream conditions ($x \to \infty$). We assume that far from the shock, the electron and ion temperatures equilibrate, so that

$$T_{i,j} = T_{e,j} \equiv T_j, \tag{7}$$

where $j \in \{0, 1\}$.

The problem statement is then:

- *Given:*
  - The upstream state $(\rho, v, T)_0$ and the upstream Mach number $M_0 = v_0/c_0$.
  - The constants γ, C_v, Z, γ_{ei} and κ_e.
  - The functions $p(\rho, T)$ and $e(\rho, T)$.
- *Calculate:*
  - The functions $\rho(x)$, $u(x)$, $T_e(x)$, and $T_i(x)$.

4 Jump Conditions

We first provide the overall jump conditions between the upstream and downstream equilibrium states at $x = \pm\infty$ and then the jump conditions at a shock.

In a reference frame where the shock speed is zero, state-$_0$ and state-$_1$ (overall jump conditions) are related by

$$\begin{pmatrix} \rho v \\ \rho v^2 + p \\ v(\rho E + p) \end{pmatrix}_0 = \begin{pmatrix} \rho v \\ \rho v^2 + p \\ v(\rho E + p) \end{pmatrix}_1 . \tag{8}$$

These equations follow from Eqs. (1a-c,7) and can be solved to find state-$_1$, given state-$_0$ and the upstream Mach number M_0 [6]. Note that Eq. (8) does not involve Eq. (1d), since the equilibrium assumption, Eq. (7), determines the final values of T_e and T_i.

The nonlinear system (1) can produce a discontinuity (an embedded hydrodynamic shock) in the flow variables, which we denote as a jump from a left state (subscript-$_L$) to a right state (subscript-$_R$). This discontinuity is governed by the shock conditions

$$\begin{pmatrix} \rho v \\ \rho v^2 + p \\ v(\rho E + p) - \kappa_e \partial_x T_e \\ -\kappa_e \partial_x T_e + \rho v T_e S_e \end{pmatrix}_L = \begin{pmatrix} \rho v \\ \rho v^2 + p \\ v(\rho E + p) - \kappa_e \partial_x T_e \\ -\kappa_e \partial_x T_e + \rho v T_e S_e \end{pmatrix}_R , \tag{9}$$

which are determined by integrating (1,6) over an infinitesimal domain surrounding the shock. Note that while T_e (for $\kappa_e \neq 0$) and ρv are continuous, $\partial_x T_e$ and S_e may be discontinuous at a shock.

5 Reduced Equations

In the steady-state, Eqs. (1a-d) simplify to

$$(\rho v)' = 0, \tag{10a}$$
$$(\rho v^2 + p)' = 0, \tag{10b}$$
$$[v(\rho E + p)]' = (\kappa_e T_e')', \tag{10c}$$
$$(\rho v e_e)' + p_e v' = \gamma_{ei}(T_i - T_e) + (\kappa_e T_e')' \tag{10d}$$

where $(\cdot)' \equiv d(\cdot)/dx$. Assuming a γ-law EOS ($p = \rho e(\gamma - 1)$), we use the analysis in Zel'dovich and Raizer [6] to simplify Equations (10(a-c)):

$$\frac{T}{T_0} = 1 + \gamma M_0^2(1-\eta)\left(\eta - \frac{1}{\gamma M_0^2}\right) = (1+\gamma M_0^2)\eta - \gamma M_0^2 \eta^2 \tag{11a}$$
$$\kappa_e \frac{dT_e}{dx} = \frac{m_0 v_0^2}{2}\frac{\gamma+1}{\gamma-1}(1-\eta)(\eta-\eta_1). \tag{11b}$$

Here $m_0 = \rho v = \rho_0 v_0$, $M_0 = v_0/c_0$ is the upstream Mach number, $\eta = v/v_0 = \rho_0/\rho$ and

$$\eta_1 = \frac{\gamma-1}{\gamma+1} + \frac{2}{\gamma+1}\frac{1}{M_0^2}.$$

We use Eq. (10d) to derive an expression for $\frac{d\eta}{dx}$. Assume $C_{v,e}$ is constant and note that

$$T_i - T_e = (Z+1)(T - T_e) \tag{12}$$

follows from the expressions in Eq. (5). Then Eq. (10d) can be written as

$$\frac{\kappa_e}{m_0 C_{v,e}}\frac{d\eta}{dx} = \frac{\frac{2(Z+1)\kappa_e\gamma_{ei}}{C_{v,e}^2 m_0^2}\frac{C_{v,e}}{v_0^2}(T - T_e) - \frac{\gamma+1}{\gamma-1}(1-\eta)(\eta-\eta_1)}{\frac{2(\gamma-1)}{\eta}\frac{C_{v,e}}{v_0^2}T_e + \frac{\gamma+1}{\gamma-1}(2\eta - (1+\eta_1))} \tag{13}$$

We now introduce some additional notation. Define the length scales $L_D = \frac{\kappa_e}{m_0 C_{v,e}}$ and $L_C = \frac{m_0 C_{v,e}}{\gamma_{ei}}$ and the scaled temperature $\Theta = \frac{C_{v,e}}{v_0^2}T$. The scaled ion and electron temperatures are defined similarly; $\Theta_{i,e} = \frac{C_{v,e}}{v_0^2}T_{i,e}$. For convenience, let $\eta_{t0} = 1 + \frac{1}{\gamma M_0^2}$ and $\mu^2 = \frac{\gamma-1}{\gamma+1}$. Note that

$$\gamma M_0^2 \Theta_0 = \frac{Z}{Z+1}\frac{1}{\gamma-1}. \tag{14}$$

We write Eqs. (11) as

$$\Theta = \frac{Z}{Z+1}\frac{1}{\gamma-1}(\eta_{t0} - \eta)\eta \tag{15}$$

and

$$L_D \frac{d\Theta_e}{dx} = \frac{1}{2\mu^2}(1-\eta)(\eta-\eta_1). \tag{16}$$

We write Eq. (13) as

$$L_D \frac{d\eta}{dx} = \frac{2(Z+1)\frac{L_D}{L_C}(\Theta - \Theta_e) - \frac{1}{\mu^2}(1-\eta)(\eta-\eta_1)}{\frac{2(\gamma-1)}{\eta}\Theta_e - \frac{2}{\mu^2}(\frac{1+\eta_1}{2} - \eta)}. \tag{17}$$

We also write Eq. (9d) as

$$(\gamma-1)\mu^2\Theta_e \log(\eta_L/\eta_R) = (\eta_L - \eta_R)\left(\frac{1+\eta_1}{2} - \frac{\eta_L + \eta_R}{2}\right), \tag{18}$$

where we have used the following formula for the entropy of an ideal electron gas

$$S_e = C_{v,e} \log(p_e \rho^{-\gamma}).$$

We use Eq. (18) to determine the jump in flow variables when a discontinuity occurs in the system of differential equations, Eqns. (16-17).

Finally, we make one additional substitution and rewrite of Eqs. (16,17). Let $\zeta = \frac{x}{2\mu^2 L_D}$ and $R = \frac{2Z}{\gamma+1}\frac{L_D}{L_C}$. Then Eq. (16) becomes

$$\frac{d\Theta_e}{d\zeta} = (1-\eta)(\eta - \eta_1) \tag{19}$$

and Eq. (17) becomes

$$\frac{d\eta}{d\zeta} = -\eta R \left(\frac{Z+1}{Z}\right) \frac{\Theta_e - \Theta_e^{c2}}{\Theta_e - \Theta_e^{c1}}. \tag{20}$$

Both Θ_e^{c1} and Θ_e^{c2} are quadratic curves in (η, Θ_e) phase space with

$$\Theta_e^{c1}(\eta) := \left(\frac{1+\eta_1}{2} - \eta\right) \frac{\eta}{\mu^2(\gamma-1)} \tag{21}$$

and

$$\Theta_e^{c2}(\eta) := \Theta - \frac{Z}{Z+1}\frac{(\eta-\eta_1)(1-\eta)}{(\gamma-1)R} = \frac{Z\left[(1-R)\eta^2 + (R\eta_{t0} - (1+\eta_1))\eta + \eta_1\right]}{(Z+1)(\gamma-1)R}. \tag{22}$$

Note that Eqs. (18,19,20) remain unchanged if the constants κ_e and γ_{ei} are replaced by the functions $\kappa_e(\rho, T_e)$ and $\gamma_{ei}(\rho, T_e)$, respectively.

6 Solution Procedure

Equations (19) and (20) form a 2×2 autonomous system of ODEs, with independent variable ζ and dependent variables η and Θ_e. Numerically integrating this system from the initial equilibrium state $(\eta, \Theta_e) = (1, \Theta_{e,0}) = (1, \Theta_0)$ to the final equilibrium state $(\eta, \Theta_e) = (\eta_1, \Theta_{e,1}) = (\eta_1, \Theta_1)$ determines the functions $\eta(\zeta)$ and $\Theta_e(\zeta)$, which ultimately determine the functions $\rho(x)$, $v(x)$, $T_e(x)$, and $T_i(x)$. However, such a direct integration is only possible while the ODEs remain continuous. Note that equation (20) has a discontinuity along the curve $\Theta_e = \Theta_e^{c1}(\eta)$. If the initial and final states are not separated by this curve, the solutions are continuous. When the initial and final states are separated by this curve, the solutions may exhibit an embedded hydrodynamic shock, depending on the value of R. This separation occurs when M_0 is greater than a critical value M_c. Above another threshold mach number, M_q, the solutions always exhibit a shock; we derive M_c and M_q in Subsection 7.2. Shocks complicate the solution procedure; when shocks occur, we integrate away from both the initial and final equilibrium states towards the discontinuity and connect the resulting numerical solutions by enforcing the shock condition, Eq. (18).

In Appendix A, we classify the initial and final equilibrium states. The initial state is always a saddle point, therefore we integrate away from state-$_0$ in the $+x$-direction. When $M_0 < M_c$, the solutions are continuous and the final state is a stable point (an attractor); we then integrate from state-$_0$ to state-$_1$. For $M_0 > M_c$, the final state is also a saddle point, so we integrate away from state-$_1$ in the $-x$-direction. In this case, the two solution curves may meet at the intersection of Θ_e^{c1} and Θ_e^{c2} and form a continuous solution, or a hydrodynamic shock will connect the two solution curves.

At state-$_0$ and state-$_1$, equations (19) and (20) are singular. To start the integration, we evaluate $d\Theta_e/d\eta$ at the end states (see Appendix B.) We then perturb η from η_j as

$$\eta_\epsilon = \eta_j + \epsilon$$

where we select $|\epsilon| \ll 1$. A simple argument ([6]) requires that Θ_e be monotone in η, so that for state-$_0$ we use $\epsilon < 0$ and for state-$_1$ we use $\epsilon > 0$. The corresponding electron temperature is

$$\Theta_{e,\epsilon} \approx \Theta_j + \epsilon \left(\frac{d\Theta_e}{d\eta} \right)_j ,$$

which is accurate to $O(\epsilon^2)$. Using $(\eta, \Theta_e)_\epsilon$ as the initial state at a freely specified spatial coordinate x_0, we then integrate Eqs. (19, 20) numerically, using an explicit Runge-Kutta scheme.

The numerical procedure may be summarized as follows:

- Determine (η_1, Θ_1) given the upstream mach number, M_0, the ideal gas constant, γ, and the ionization number, Z.
- Determine M_c and M_q. See Subsection 7.2.
- If $M_0 <= M_c$
  - evaluate $d\Theta_e/d\eta$ at $\eta = 1$
  - determine $\Theta_{e,\epsilon}$
  - integrate from starting state $(\eta, \Theta_e)_\epsilon$ near $(1, \Theta_0)$ to an end state near (η_1, Θ_1) in the $+x$-direction
- If $M_c < M_0 < M_q$
  - evaluate $d\Theta_e/d\eta$ at $\eta = 1$ and $\eta = \eta_1$
  - determine $\Theta_{e,\epsilon}$ at both end states
  - integrate from a starting state $(\eta, \Theta_e)_\epsilon$ near $(1, \Theta_0)$ in the $+x$-direction
  - integrate from a starting state $(\eta, \Theta_e)_\epsilon$ near (η_1, Θ_1) in the $-x$-direction
  - if the two solution curves intersect at the intersection of Θ_e^{c1} and Θ_e^{c2}, note the value of Θ_e at this intersection.
  - otherwise, a hydrodynamic shock connects the two solution curves, which have intersecting Θ_e ranges. Use the method of false position (Newton's Method without derivative evaluations) to find a value of Θ_e (and corresponding η_L and η_R) that satisfies the shock condition, Eq. (18).
  - Translate the state-$_1$ solution curve so that the solution curves intersect at the resulting value of Θ_e.
- If $M_q < M_0$
  - evaluate $d\Theta_e/d\eta$ at $\eta = 1$ and $\eta = \eta_1$
  - determine $\Theta_{e,\epsilon}$ at both end states
  - integrate from a starting state $(\eta, \Theta_e)_\epsilon$ near $(1, \Theta_0)$ in the $+x$-direction
  - integrate from a starting state $(\eta, \Theta_e)_\epsilon$ near (η_1, Θ_1) in the $-x$-direction
  - a hydrodynamic shock connects the two solution curves, which have intersecting Θ_e ranges. Use the method of false position (Newton's Method without derivative evaluations) to find a value of Θ_e (and corresponding η_L and η_R) that satisfies the shock condition, Eq. (18).
  - Translate the state-$_1$ solution curve so that the solution curves intersect at the resulting value of Θ_e.

7 Results

In this section, we present several example solutions. Upon initial inspection it appears that three parameters, γ_{ei}, κ_e and M_0, influence the classification of possible solutions. The electron ion coupling term, γ_{ei} appears in Eqs. (20) through the length scale ratio, R. The electron thermal diffusivity, κ_e, appears (through L_D) in both R and the scaled independent variable, ζ, which determines the integration length scale. Thus, for fixed values of M_0 and R, varying κ_e will produce a range of self-similar solutions differing only by length scale, i.e., qualitatively different solutions will not be produced. Therefore, only the two parameters, M_0 and R, determine the qualitative solution behavior. The upstream mach number, M_0, determines the strength of the flow, while R determines how strongly the ion and electron temperatures couple. For $R \gg 1$, the electron and ion temperatures are strongly coupled, while for $R \ll 1$, the electron and ion temperatures are weakly coupled. We will refer to solutions with $R \gg 1$ as strongly coupled, and solutions with $R \ll 1$ as weakly coupled.

For the solutions presented below, we provide both temperature profiles (plots of T_e and T_i versus x) and the corresponding (η, Θ) phase space diagrams. We use $\rho_0 = 1$, $u_0 = 0$, $\gamma = 5/3$, $Z = 1$, $C_v = 2$ (so that $C_{v,e} = C_{v,i} = 1$) and $p_0 = \gamma^{-1} = 3/5$ (so that $c_0 = 1$ and $m_0 = \rho_0 v_0 = M_0$). We fix $\kappa_e = 1$ so that the integration length scale depends only on M_0. With these settings, the value of M_0 below which solutions are continuous, regarless of the value of R, is $M_c \approx 1.125$ and the value of M_0 above which solutions are discontinuous, regardless of the value of R, is $M_q \approx 1.661$. We then vary M_0 and $R = \frac{3\gamma_{ei}}{4M_0^2}$ to explore the range of possible solutions. Figure (1) indicates the values of M_0 and R that we present.

In Figures (2-4), we present three continuous solutions with upstream Mach number $M_0 = 1.1$ and varying values of the length scale ratio, R. The solutions are continuous because the initial and final states are not separated in phase space by the curve $\Theta_e = \Theta_e^{c1}(\eta)$, along which $\frac{d\eta}{dx}$ is discontinuous. Note that in each case, $\Theta_e > \Theta_i$ upstream, but the phase space curves intersect and $\Theta_i > \Theta_e$ downstream. Since $\frac{d\eta}{dx} < 0$ throughout the solution and $\Theta_e > \Theta_e^{c1}$, we also have the inequality $\Theta_e > \Theta_e^{c2}$, but note that Θ_e approaches Θ_e^{c2} near the final state, particularly evident in Figure (2). This limiting behavior suggests that for continuous solutions, Θ_e^{c2} serves as a lower bound for Θ_e near the final equilibrium state. Note that in Figure (2), $\Theta_i(\eta)$ is not monotone and a peak occurs in $T_i(x)$. As R increases, Θ_e^{c2} approaches Θ and the electron and ion temperatures become strongly coupled. At $R = 10.0$, the coupling of the temperatures is such that the differences in the temperatures are imperceptible in the profile and phase space diagrams.

In Figures (5-10), we present four solutions with upstream Mach number $M_0 = 1.4$ and varying values of the length scale ratio, R. In each of these solutions, the initial and final states in phase space are separated by the curve $\Theta_e = \Theta_e^{c1}(\eta)$, however not all of the solutions are discontinuous. In Figures (5-7), a hydrodynamic shock connects the Θ_e solution curves; in phase space, the shock causes Θ_e to cross both Θ_e^{c1} and Θ_e^{c2}, so that $\frac{d\eta}{dx} < 0$ throughout the solution. Again, we have $\Theta_e > \Theta_i$ near the upstream state and $\Theta_i > \Theta_e$ near the downstream state. We also note that $\Theta_i(\eta)$ is not monotone and a peak occurs in $T_i(x)$. Note that for $R = 0.1$ and $R = 1.0$, the peak in $T_i(x)$ occurs at the hydrodynamic shock, while for $R = 10.0$, the peak occurs downstream of the shock. We investigate the occurence of this post–shock maximum in Subsection 7.1. This behavior is reminiscent of a Zel'dovich spike [6]. In Figure (9), a continuous solution exists, despite the separation of the initial and final states by the curve $\Theta_e = \Theta_e^{c1}$. The continuity of the solution is possible because Θ_e passes through the intersection of Θ_e^{c1} and Θ_e^{c2}. We describe the boundary between continuous and discontinuous solutions in Subsection 7.2.

In Figures (11-13), we present three solutions with upstream Mach number $M_0 = 1.7$ and varying values of the length scale ratio, R. In each of these solutions, the initial and final states in phase space are separated by the curve $\Theta_e = \Theta_e^{c1}(\eta)$ and each solution contains an embedded hydrodynamic shock. Note that in the phase space diagrams, the intersection of Θ and Θ_e^{c1} occurs at a value of $\Theta_e > \Theta_1$. As R increases, Θ_e^{c2} approaches Θ, and so the intersection of Θ_e^{c1} and Θ_e^{c2} approaches the intersection of Θ_e^{c1} and Θ. Since this intersection occurs at $\Theta_e > \Theta_1$ and $\frac{d\Theta_e}{d\eta} < 0$, the solution curves can not meet at the intersection of Θ_e^{c1} and Θ_e^{c2} for large values of R. For smaller values of R where the intersection of Θ_e^{c1} and Θ_e^{c2} may occur in the rectangle $[\eta_1, 1] \times [\Theta_0, \Theta_1]$, the solution branches do not approach the intersection.

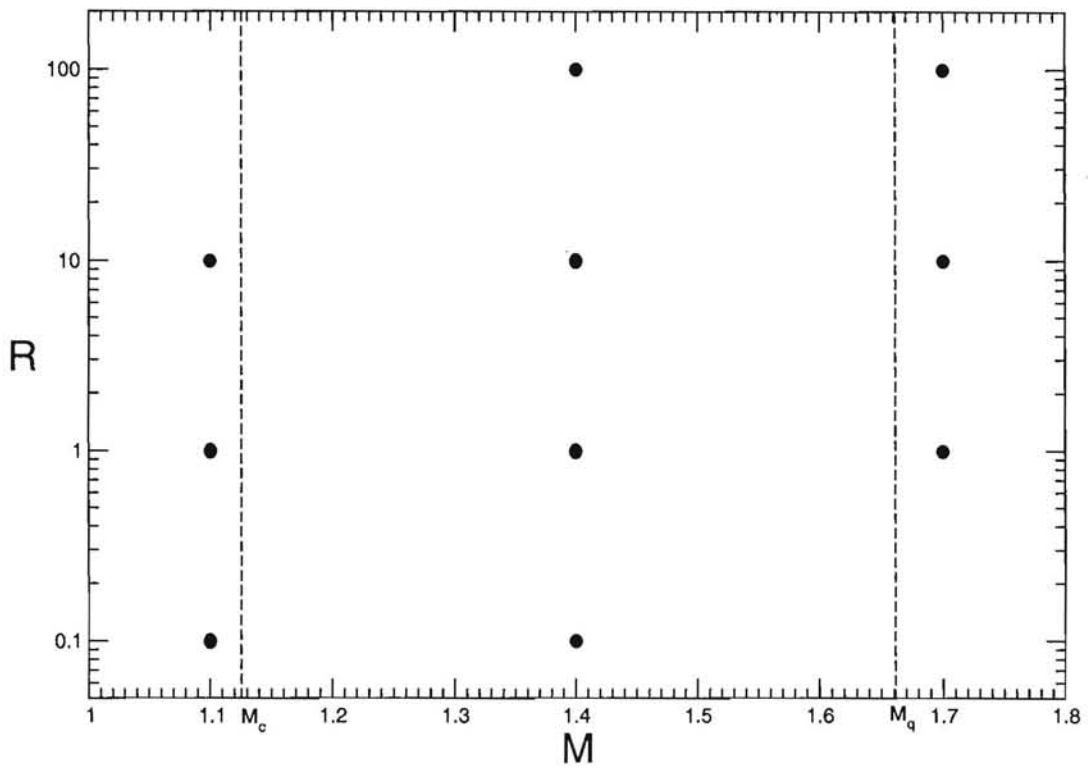

Figure 1: Solution Parameter Space. M_c is the cutoff in the upstream mach number, M_0, such that for any value of $M_0 < M_c$ the solutions will be continuous. For $M_c < M_0 < M_q$, hydrodynamic shocks may appear in the solutions, depending on the value of R. For $M_0 > M_q$, hydrodynamic shocks appear in the solutions, regardless of the value of R. For $R \gg 1$, the electron and ion temperatures are strongly coupled. For $R \ll 1$, the temperatures are weakly coupled. Points indicate solutions presented below.

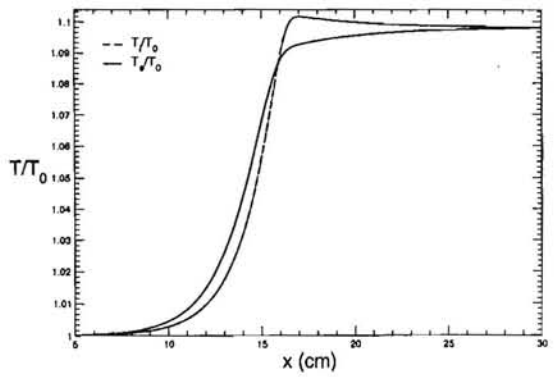

(a) Temperature Profiles

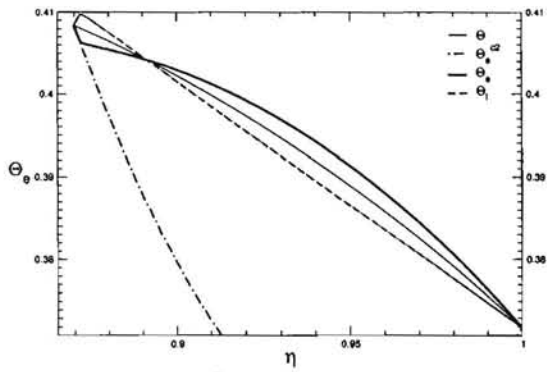

(b) Solutions in Phase Space

Figure 2: Continuous Solution with Weak Coupling. $M_0 = 1.10$ and $R = 0.1$.

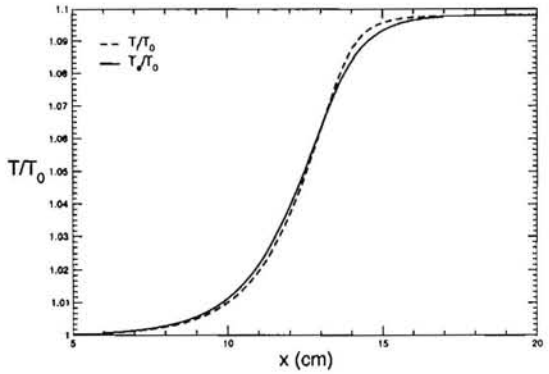

(a) Temperature Profiles

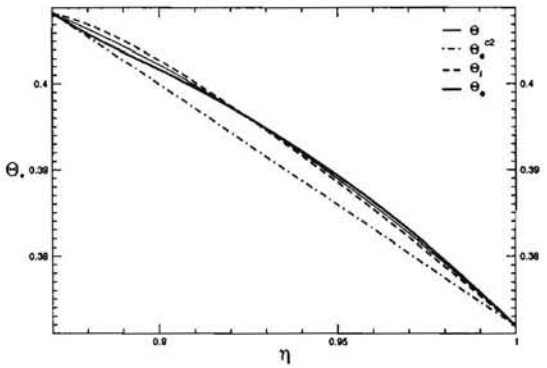

(b) Solutions in Phase Space

Figure 3: Continuous Solution with Moderate Coupling. $M_0 = 1.10$ and $R = 1.0$.

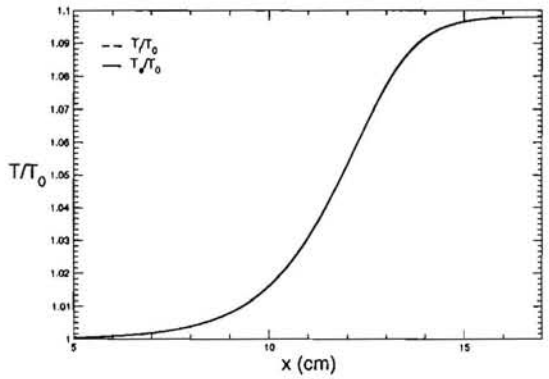

(a) Temperature Profiles

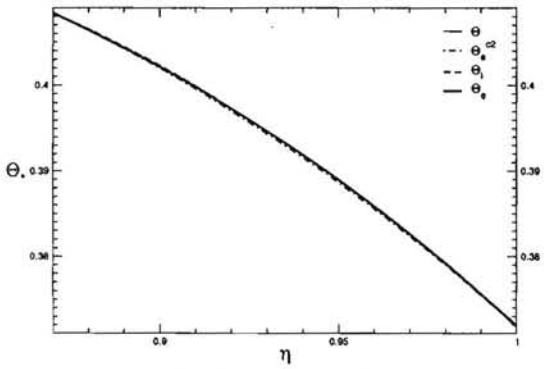

(b) Solutions in Phase Space

Figure 4: Continuous Solution with Strong Coupling. $M_0 = 1.10$ and $R = 10.0$.

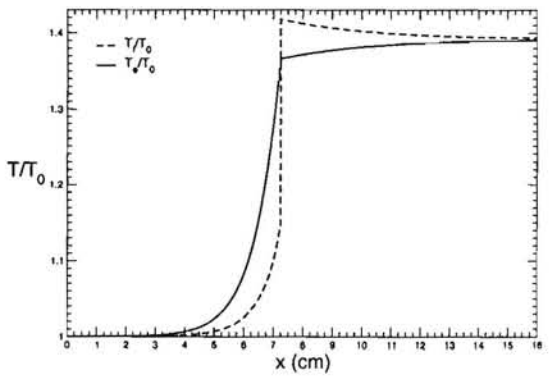

(a) Temperature Profiles

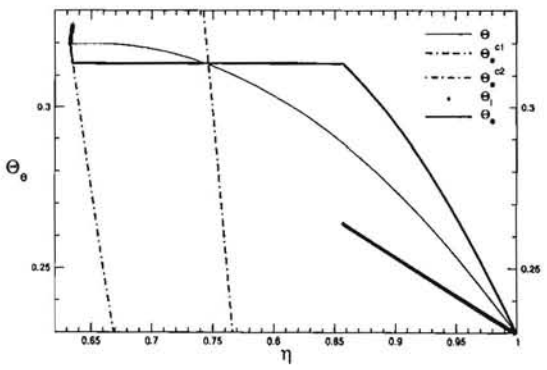

(b) Solutions in Phase Space

Figure 5: Discontinuous Solution with Weak Coupling. $M_0 = 1.40$ and $R = 0.1$.

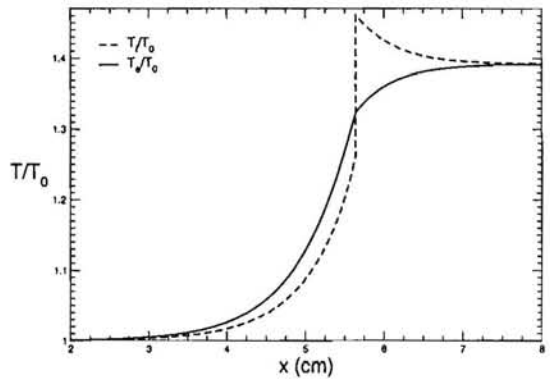

(a) Temperature Profiles

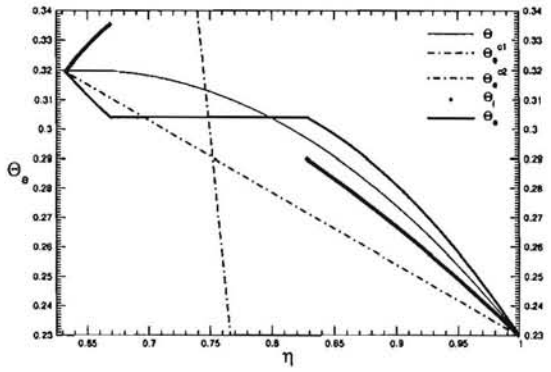

(b) Solutions in Phase Space

Figure 6: Discontinuous Solution with Moderate Coupling. $M_0 = 1.40$ and $R = 1.0$.

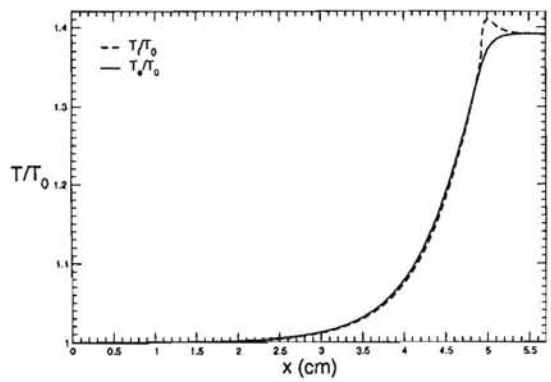

(a) Temperature Profiles

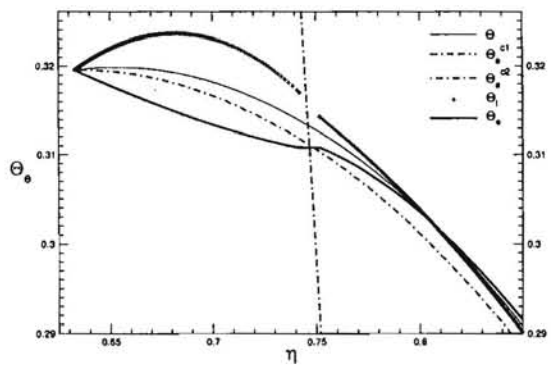

(b) Solutions in Phase Space

Figure 7: Discontinuous Solution with Strong Coupling. $M_0 = 1.40$ and $R = 10.0$.

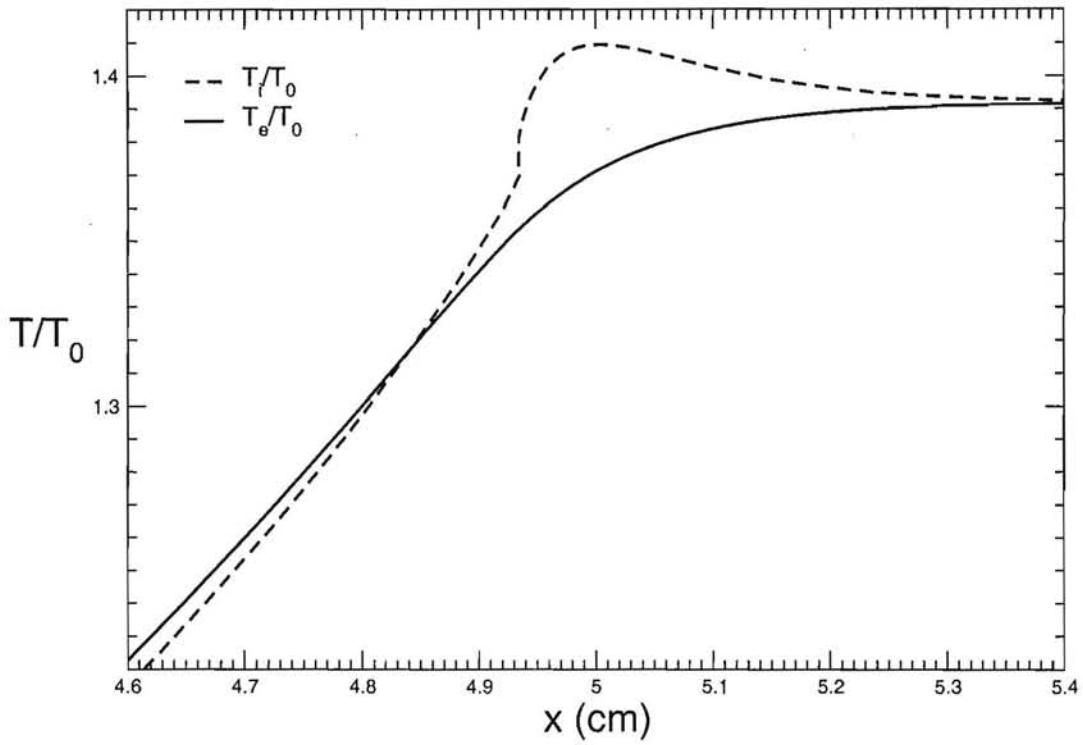

Figure 8: Discontinuous Solution with Strong Coupling. $M_0 = 1.40$ and $R = 10.0$. Zoom on hydro shock. Note peak in T_i is downstream of the hydro shock.

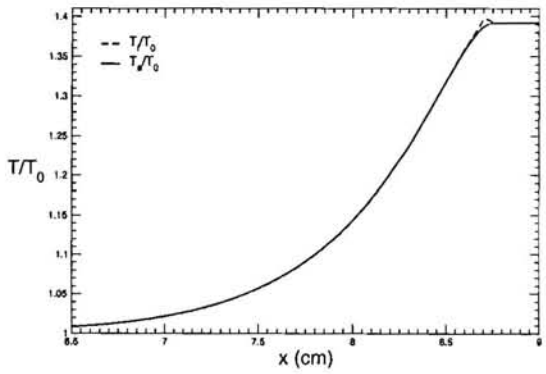

(a) Temperature Profiles

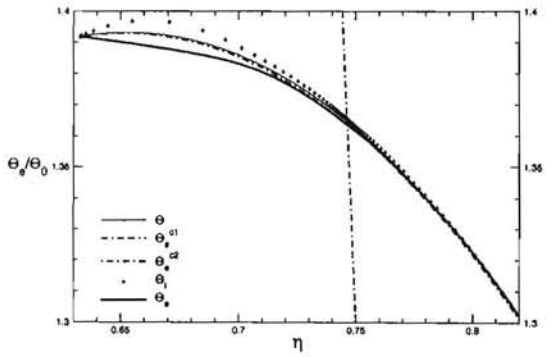

(b) Solutions in Phase Space

Figure 9: Continuous Solution with Strong Coupling. $M_0 = 1.40$ and $R = 100.0$.

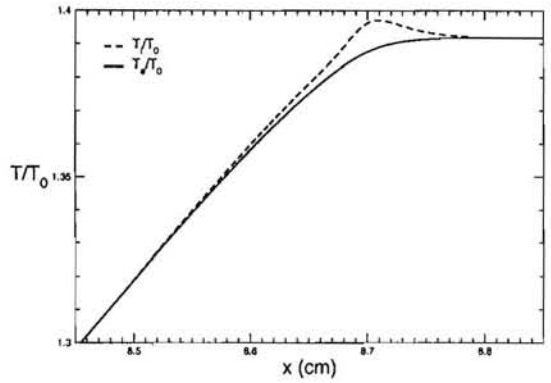

(a) Temperature Profiles

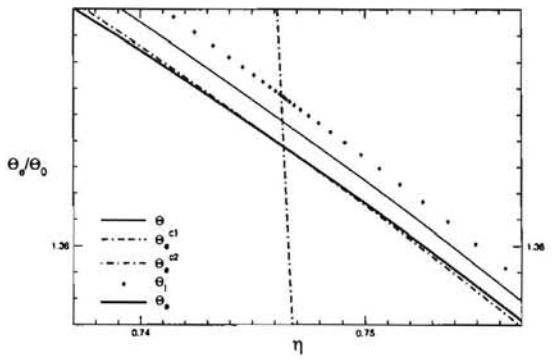

(b) Solutions in Phase Space

Figure 10: Continuous Solution with Strong Coupling. $M_0 = 1.40$ and $R = 100.0$. Zoom on removable singularity of $\frac{d\eta}{d\zeta}$.

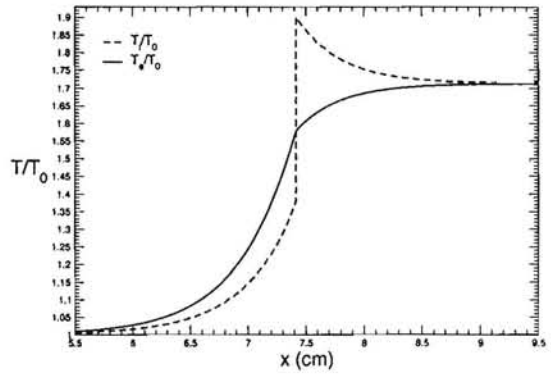

(a) Temperature Profiles

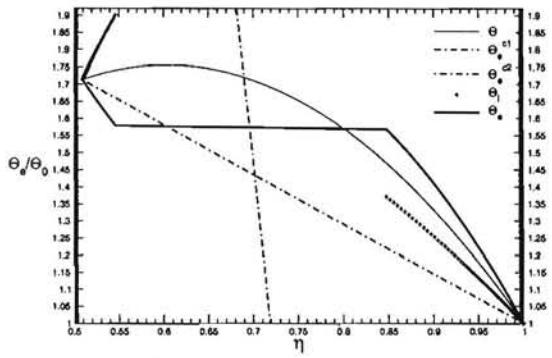

(b) Solutions in Phase Space

Figure 11: Discontinuous Solution with Moderate Coupling. $M_0 = 1.70$ and $R = 1.0$.

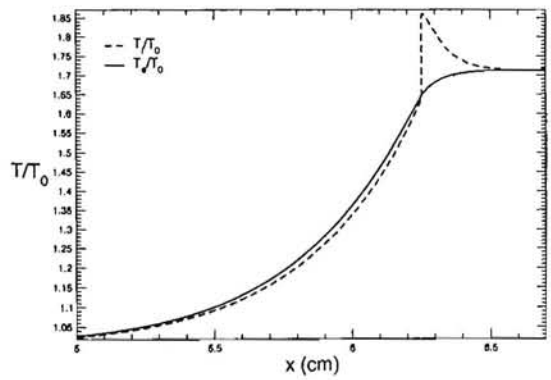

(a) Temperature Profiles

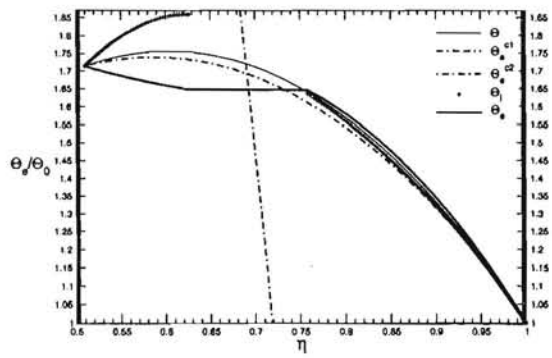

(b) Solutions in Phase Space

Figure 12: Discontinuous Solution with Strong Coupling. $M_0 = 1.70$ and $R = 10.0$.

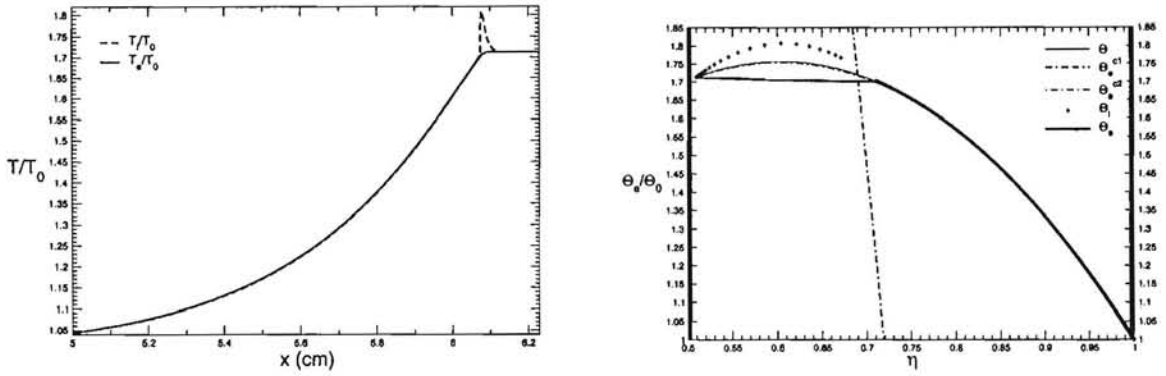

(a) Temperature Profiles

(b) Solutions in Phase Space

Figure 13: Discontinuous Solution with Strong Coupling. $M_0 = 1.70$ and $R = 100.0$.

7.1 Maximum Ion Temperature

In this section, we explain why a maximum in the ion temperature, T_i, can occur in the post-shock relaxation region. Differentiating Eq. (12) provides a simple condition for when $dT_i/dx = 0$:

$$(Z+1)\frac{dT}{dx} = Z\frac{dT_e}{dx}.$$

In (η, Θ_e) phase space, this condition translates to

$$(Z+1)\frac{d\Theta}{d\eta} = Z\frac{d\Theta_e}{d\eta}.$$

Since $d\Theta_e/d\eta < 0$, a maximum in the ion temperature can only occur when $d\Theta/d\eta < 0$. Thus, by differentiating Eq. (15), we derive a necessary condition for the formation of a maximum ion temperature:

$$\eta > \eta_{t0}/2.$$

Consider the hydrodynamic shock in the phase space diagrams, Figures (5–7(b)). Let η_s be the value of η on the downstream (left in the phase space diagrams) side of the shock and let η_{pc} be value of η on the upstream (right) side of the shock. The necessary condition for a maximum in the ion temperature to occur in the post-shock relaxation region is then:

$$\eta_s > \eta_{t0}/2. \tag{23}$$

With $\gamma = 5/3$ and $M_0 = 1.4$, as in Figures (5-7), $\eta_{t0}/2 \approx 0.65$. In both Figure (6(b)) and Figure (7(b)), $\eta_s > \eta_{t0}/2$. However, the ion temperature passes through a post–shock maximum only in Figure (7(b)).

The condition in Equation (23) can be expressed alternatively in terms of the local Mach number, M, of the flow. The local Mach number is given by

$$M = \frac{v}{c} = M_0\eta\left(\frac{T_0}{T}\right)^{-1/2} = \sqrt{\frac{\eta/\gamma}{\eta_{t0}-\eta}}. \tag{24}$$

We substitute η_1, η_s, η_{pc} and $\eta = 1$ into Equation (24) to obtain the associated terms M_1, M_s, M_{pc} and M_0. We use the expression $M_{1,c}$ to denote the value of M_1 when $M_0 = M_c$. When $\eta = \eta_{t0}/2$, $M = M_{ISP}$ where

$$M_{ISP} = \frac{1}{\sqrt{\gamma}}$$

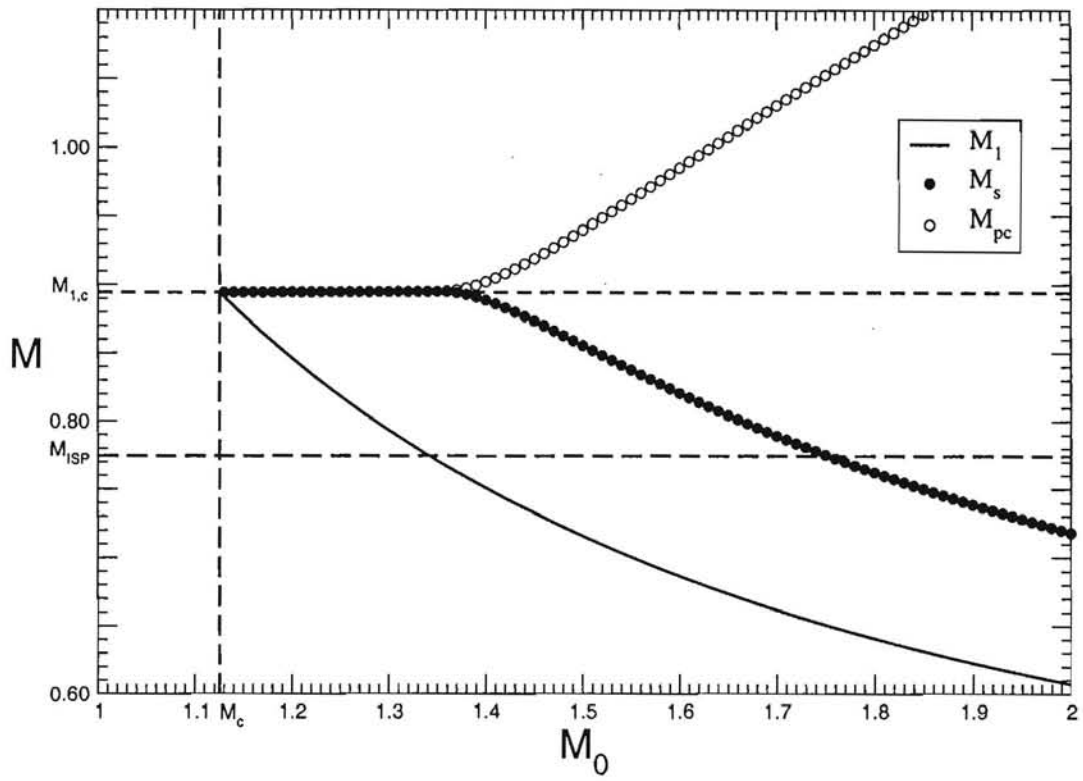

Figure 14: Plots of M_1, M_s and M_{pc} versus M_0 for $\gamma_{ei} = 26.13$. $R = 10.0$ at $M_0 = 1.4$.

is the isothermal sonic point. With $Z = 1$ and $\gamma = 5/3$, $M_{ISP} \approx 0.7746$ and $M_{1,c} \approx 0.8944$. Recall that in steady solutions of the Euler equations with material heat conduction, values of M_0 larger than M_{ISP} result in an isothermal shock [6]. Equation (23) is expressed as

$$M_s > M_{ISP}.$$

In Figure (14), we plot M_1, M_s and M_{pc} as functions of M_0 for a fixed value of γ_{ei}. Note that M_s and M_{pc} are not applicable for continuous solutions with $M_0 < M_c$. At $M_0 = 1.4$, $M_s > M_{ISP} > M_1$ and the jump from M_s to M_{pc} is small relative to the difference in M_0 and M_1; most of the compression that occurs between the far upstream and downstream states is not due to the hydrodynamic shock.

Physically, the presence of electron heat conduction and electron–ion coupling serve to weaken the hydrodynamic shocks that occur in the solutions. Note that the quantity R is proportional to the product $\kappa_e \gamma_{ei}$, so that for positive $R \ll 1$ the diffusion and relaxation effects are minor and the hydrodynamic shock is responsible for most of the compression in the solutions. When $R \gg 1$, significant continuous compression occurs in both the precursor and relaxation regions and not at the shock. A maximum ion temperature occurs in the relaxation region when the energy flowing into the ions from the compression is balanced by the energy flowing from the ions into the electrons. These extrema are only possible when $\kappa_e \neq 0$, which results in regions of continuous compression.

7.2 Boundary Between Continuous and Discontinuous Solutions

We combine Eqn. (19,20) to determine a first order differential equation for $\Theta_e = \Theta_e(\eta)$.

$$\frac{d\Theta_e}{d\eta} = -\frac{(1-\eta)(\eta-\eta_1)}{\eta R\,(1+Z^{-1})}\,\frac{\Theta_e - \Theta_e^{c1}}{\Theta_e - \Theta_e^{c2}} \tag{25}$$

Imshennik [2] integrated this differential equation for nonlinear $\kappa_e = \kappa_e(\rho, T_e)$ and $\gamma_{ei} = \gamma_{ei}(\rho, T_e)$ and used this equation to derive the boundary between continuous and discontinuous solutions. However, that derivation failed to consider a possibility that complicates this boundary.

The only solutions to Eq. (25) that are physically realizable [6] satisfy

$$\frac{d\Theta_e}{d\eta} < 0. \tag{26}$$

Note that the right hand side of Eq. (25) changes sign along the two quadratic curves $\Theta_e = \Theta_e^{c1}(\eta)$ and $\Theta_e = \Theta_e^{c2}(\eta)$. The existence of continuous or discontinuous solutions then depends largely upon the arrangement of the far upstream and downstream states ($(1,\Theta_0)$ and (η_1,Θ_1), respectively) with respect to these two quadratic curves in (η,Θ_e) phase space.

Imshennik derived the boundary between continuous and discontinuous solution behavior by solving for the conditions under which the far downstream state, (η_1,Θ_1), lies on the curve $\Theta_e = \Theta_e^{c1}(\eta)$. We do this here in two steps. First we use Eqs. (15,21) to solve for the value of η where $\Theta = \Theta_e^{c1}$,

$$\eta_c = \left(1 + \frac{1}{\gamma M_0^2}\right)\frac{Z+\gamma}{2Z+\gamma+1}.$$

We then set $\eta_c = \eta_1$ to arrive at a condition on M_0, the upstream Mach number. Let

$$M_c = \left[\frac{1}{\gamma}\frac{\gamma^2 + (3Z+1)\gamma - Z}{(3Z+1) - \gamma(Z-1)}\right]^{1/2}$$

and note that

$$\lim_{Z\to\infty} M_c = M_* = \left(\frac{1}{\gamma}\frac{3\gamma-1}{3-\gamma}\right)^{1/2}.$$

We add that M_* is the cut-off between continuous and discontinuous solutions in the simpler case of hydrodynamic flow with material heat conduction [6]. Also note that for all values of Z, $M_c < M_*$; for $Z = 1$ and $\gamma = 5/3$, $M_c \approx 1.125$ and $M_* \approx 1.342$. For $M_0 < M_c$, the far upstream and downstream states are always above the curve $\Theta_e = \Theta_e^{c1}(\eta)$ and the solutions proceed continuously from the upstream state to the downstream state. For $M_0 > M_c$, the states $(1,\Theta_0)$ and (η_1,Θ_1) are separated by the curve $\Theta_e = \Theta_e^{c1}(\eta)$. Imshennik claimed that this separation necessitated discontinuous solutions. However, this overlooks the possibility that $\Theta_e^{c1}(\eta)$ and Θ_e^{c2} might intersect in the rectangle $[\eta_1,1]\times[\Theta_0,\Theta_1]$ and that the solution curves that pass through the far upstream and downstream states might also pass continuously through this intersection. Figures (9-10) present an example of such a continuous solution.

We now assume that $M_0 > M_c$ and investigate the true boundary between continuous and discontinuous solutions. For $M_0 > M_c$ the far upstream and downstream states are separated by the curve $\Theta_e = \Theta_e^{c1}(\eta)$. Since the curve $\Theta_e = \Theta_e^{c2}(\eta)$ passes through the far upstream and downstream states, Θ_e^{c1} and Θ_e^{c2} have an intersection for a value of η between η_1 and 1. For R sufficiently small, this intersection occurs at a value of Θ_e less than Θ_0; hence, this intersection is inaccessible for solutions that pass through (η_1,Θ_1) and $(1,\Theta_0)$ and satisfy Eq. (26). In this case, an embedded hydrodynamic shock connects the two solution curves that pass through the far upstream and downstream states. As R increases, the intersection of Θ_e^{c1} and Θ_e^{c2} enters the rectangle $[\eta_1,1]\times[\Theta_0,\Theta_1]$; it then becomes possible for solutions to pass continously from the far upstream state $(1,\Theta_0)$ through the intersection and to the far downstream state (η_1,Θ_1). In this case, the

continuity of the solution depends on whether the solution curves pass through this intersection; we have not found a simple condition that quantifies the conditions for the solutions to pass through this intersection.

In the limit $R \rightarrow \infty$, $\Theta_e^{c2} \rightarrow \Theta$, so that the intersection of Θ_e^{c1} and Θ_e^{c2} approaches the intersection of Θ_e^{c1} and Θ. We then have two possibilities for large values of R. Depending upon the upstream mach number M_0, the intersection of Θ_e^{c1} and Θ will either have $\Theta_e > \Theta_1$ or $\Theta_e <= \Theta_1$. For $M_c < M_0 < M_*$, the intersection of Θ_e^{c1} and Θ will have $\Theta_e < \Theta_1$, by definition of M_*; see Zel'dovich [6]. For $M_0 > M_*$, $\Theta = \Theta_1$ has two solutions; one at $\eta = \eta_1$ and the other at $\eta = \eta_{t0} - \eta_1 > \eta_1$. We then set $\eta_c = \eta_{t0} - \eta_1$, to determine the value of $M_0 > M_*$ where $\Theta_e^{c1} = \Theta = \Theta_1$ and $\eta > \eta_1$. Let

$$M_q = \left[\frac{1}{\gamma}\frac{(3\gamma-1)Z + (\gamma+1)(2\gamma-1)}{(3-\gamma)Z + (\gamma+1)(2-\gamma)}\right]^{1/2}$$

and note that

$$\lim_{Z\rightarrow\infty} M_q = M_*.$$

Note further that for all values of Z, $M_q > M_*$; for $Z = 1$ and $\gamma = 5/3$, $M_q \approx 1.661$. For $M_0 > M_q$, the intersection of Θ_e^{c1} and Θ will have $\Theta_e > \Theta_1$, while for $M_0 < M_q$, the intersection will have $\Theta_e < \Theta_1$. For $M_c < M_0 < M_q$ and R sufficiently large, the intersection of Θ_e^{c1} and Θ_e^{c2} will satisfy $\Theta_e < \Theta_1$ and therefore be accessible to continuous solution curves that pass through both the far upstream and downstream states. The numerical results above suggest that for a fixed value of M_0 with $M_c < M_0 < M_q$, the solutions are always continuous for R greater than some value that depends nontrivially on M_0. For $M_q < M_0$, the intersection of Θ_e^{c1} and Θ_e^{c2} will only satisfy $\Theta_0 < \Theta_e < \Theta_1$ for R in a range of values that contains $R = 1$. The numerical results above suggest that for a fixed value of M_0 with $M_q < M_0$, the solutions are never continuous. We hypothesize that the boundary between continuous and discontinuous solutions is a curve $R = R_c(M_0)$ in the (M_0, R) plane that begins near $(M_c, 0)$ and increases monotonically with

$$\lim_{M_0\rightarrow M_q} R_c(M_0) = \infty.$$

8 Conclusion

We have developed solutions for a simple model of shocks in a fully ionized plasma. These solutions capture the essential elements of plasma shocks: electron preheating in the region upstream of the shock and electron-ion relaxation in the downstream region. As predicted by Imshennik, for weak enough flows, fully continuous solutions occur; while for stronger flows, the solutions exhibit embedded hydrodynamic shocks. In contrast with Imshennik, we find that the boundary between continuous and discontinuous solutions is not independent of the electron diffusivity, κ_e, or γ_{ei}, the electron–ion coupling parameter. The character of the solutions is largely dependent on two terms: the upstream Mach number M_0 and a term R that is proportional to $\frac{\kappa_e\gamma_{ei}}{M_0^2}$. Below the critical Mach number derived by Imshennik, continuous solutions emerge from our model. However, continuous solutions are still possible above that threshold Mach number, if the term R is large enough. For discontinuous solutions that occur near the boundary between continuous and discontinuous solutions, the ion temperature may continue to increase and achieve a maximum in the post–shock relaxation region. This observation of a post–shock maximum temperature is similar to an effect seen in radiating flows [3].

The assumption of constant electron diffusivity and electron–ion coupling terms simplifies the analysis of this model. However, using a more realistic model of these terms would not impose additional difficulties on the numerical integration of the system of differential equations that govern this model. This model could also be used to verify the treatment of the electron diffusivity with flux limiters. A more serious restriction of our model is the assumption of an ideal gas equation of state and the subsequent splitting of specific internal energy and pressure into electron and ion components. A more general EOS, for both the electrons and the ions, should be the subject of future work.

While we have shown that the boundary between continuous and discontinuous solutions does depend on the electron diffusivity and the electron–ion coupling parameter, calculation of precise conditions for the existence of an embedded shock are left for a future work. In each discontinuous solution we have considered, we have always been able to connect the two solution branches with an embedded hydrodynamic shock by finding points on both branches that satisfy the shock condition. An interesting mathematical question would be to prove the general existence and uniqueness of the solutions with embedded hydrodynamic shocks. Finally, our work complements previous models of two–temperature (material and radiation) radiating flows; combining these models and investigating simple three–temperature (electron, ion and radiation) models seems like a natural progression of this work.

References

[1] R. P. Drake. Theory of radiative shocks in optically thick media. *Physics of Plasmas*, 14:043301, 2007.

[2] V. S. Imshennik. Shock wave structure in a dense high–temperature plasma. *Soviet Physics JETP*, 15(1):167–174, 1962.

[3] R. B. Lowrie and J. D. Edwards. Radiative shock solutions with grey nonequilibrium diffusion. *Shock Waves*, 18(2):129–143, 2008.

[4] V. D. Shafranov. The structure of shock waves in a plasma. *Soviet Physics JETP*, 5(6):1183–1188, 1957.

[5] Y. B. Zel'dovich. Shock waves of large amplitude in air. *Soviet Physics JETP*, 5(5):919–927, 1957.

[6] Y. B. Zel'dovich and Y. P. Raizer. *Physics of Shock Waves and High-Temperature Hydrodynamic Phenomena*. Dover, 2002.

A Stationary Points

Equations (19,20) form a 2×2 autonomous system of ODEs. The system has two stationary points in (η, Θ_e) space: $(1, \Theta_0)$ and (η_1, Θ_1); In order to numerically integrate this system, it is useful to classify these stationary points.

We write the system Eqn. (19,20) as

$$\frac{d\eta}{d\zeta} = f(\eta, \Theta_e) \tag{27}$$

$$\frac{d\Theta_e}{d\zeta} = g(\eta) \tag{28}$$

We linearize the system above near a stationary point $p = (\eta_p, \Theta_p)$ to obtain a system of the form $\partial_\zeta \vec{y} = A\vec{y}$, where $\vec{y} = (\eta - \eta_p, \Theta_e - \Theta_p)^T$ and

$$A = \begin{pmatrix} \partial_\eta f(p) & \partial_{\Theta_e} f(p) \\ \partial_\eta g(p) & 0 \end{pmatrix}.$$

The eigenvalues of A are

$$\lambda_\pm = \frac{\partial_\eta f}{2}\left[1 \pm \sqrt{1 + 4\frac{\partial_\eta g \partial_{\Theta_e} f}{(\partial_\eta f)^2}}\right]$$

We write $\partial_\eta g$ as

$$\partial_\eta g = [(1 - \eta) - (\eta - \eta_1)]$$

and note that at $\eta = 1$, $\partial_\eta g < 0$ and at $\eta = \eta_1$, $\partial_\eta g > 0$. We write $\partial_{\Theta_e} f$ as

$$\partial_{\Theta_e} f = -\eta R\left(1 + Z^{-1}\right)\frac{\Theta_e^{c2}(\eta) - \Theta_e^{c1}(\eta)}{(\Theta_e - \Theta_e^{c1}(\eta))^2}$$

and note that $\Theta_e^{c2}(1) = \Theta_0$ and $\Theta_e^{c2}(\eta_1) = \Theta_1$. Evaluating this derivative at the stationary points leads to the following inequalities:

$$\partial_{\Theta_e} f(1, \Theta_0) = -\frac{R\left(1 + Z^{-1}\right)}{\Theta_e^{c1}(1) - \Theta_0} < 0$$

and

$$\partial_{\Theta_e} f(\eta_1, \Theta_1) = -\frac{\eta_1 R\left(1 + Z^{-1}\right)}{\Theta_e^{c1}(\eta_1) - \Theta_1},$$

which is negative for $M_0 < M_c$ and positive for $M_0 > M_c$.

We now have enough information to classify the stationary point $(1, \Theta_0)$. At this point, $\partial_\eta g < 0$ and $\partial_{\Theta_e} f < 0$. Hence $\lambda_+\lambda_- < 0$ and so $(1, \Theta_0)$ is a saddle point. We can also classify the point (η_1, Θ_1) in the case of $M_0 > M_c$. In that case, we have $\partial_\eta g > 0$ and $\partial_{\Theta_e} f > 0$. Again, $\lambda_+\lambda_- < 0$ and so (η_1, Θ_1) is a saddle point for flows with $M_0 > M_c$.

In the case of flows with $M_0 < M_c$, we must consider both the sign of $\partial_\eta f$ and the sign of the discriminant

$$\Delta^2 = f_\eta^2 + 4 g_\eta f_{\Theta_e}$$

to classify (η_1, Θ_1). We evaluate $\partial_\eta f$ at this stationary point

$$\partial_\eta f(\eta_1, \Theta_1) = \eta_1 R\left(1 + Z^{-1}\right)\left[\frac{\partial_\eta \Theta_e^{c2}(\eta_1)}{\Theta_1 - \Theta_e^{c1}(\eta_1)}\right]$$

For $M_0 < M_c$, the $\partial_\eta \Theta_e^{c2}(\eta_1)$ term in the numerator above is negative and the denominator is positive. Hence, for $M_0 < M_c$, $\partial_\eta f(\eta_1, \Theta_1) < 0$. The discriminant can be written as

$$\Delta^2 = \left(\frac{\eta_1}{\gamma - 1}\right)^2 \left[\frac{R(\eta_{t0} - 2\eta_1) - (1 - \eta_1)}{\Theta_1 - \Theta_e^{c1}(\eta_1)}\right]^2 - 4\frac{\eta_1(1 - \eta_1)R(1 + Z^{-1})}{\Theta_1 - \Theta_e^{c1}(\eta_1)},$$

which after a non–trivial amount of algebra can be expressed as

$$\left(\frac{\gamma - 1}{\eta_1}\right)^2 \left[\Theta_1 - \Theta_e^{c1}(\eta_1)\right]^2 \Delta^2 = \left[R(\eta_{t0} - 2\eta_1) + (1 - \eta_1)\right]^2 + 2R(1 - \eta_1)^2 Z^{-1}(\gamma + 1) > 0.$$

Since the discriminant is positive, the eigenvalues are both real; the other derivative evaluations above imply that the eigenvalues are both negative. Hence (η_1, Θ_1) is a stable point for $M_0 < M_c$.

B Limit Calculations

B.1 $\eta = 1$

We now calculate the limit

$$\lim_{\eta \to 1} \frac{d\Theta_e}{d\eta}$$

and show that near $\eta = 1$, $\Theta_e > \Theta$. First, we write Eq. (25) as

$$-\frac{\eta/(\gamma - 1)}{\Theta_e - \Theta_e^{c1}(\eta)} \frac{d\Theta_e}{d\eta} = \frac{1}{1 + (\gamma - 1)R(1 + Z^{-1})\frac{\Theta_e - \Theta}{(1 - \eta)(\eta - \eta_1)}} \tag{29}$$

Then we use the first order approximations near $\eta = 1$

$$\Theta_* \approx \Theta_0 + \left(\lim_{\eta \to 1} \frac{d\Theta_*}{d\eta}\right)(\eta - 1)$$

to calculate

$$\Theta_e - \Theta \approx \left[\lim_{\eta\to 1}\frac{d\Theta_e}{d\eta} - \frac{d\Theta}{d\eta}(1)\right](\eta - 1).$$

We then have a quadratic equation for the desired limit:

$$-ax = \frac{1}{1 - b(x - c)}$$

which has the solutions

$$x_\pm = \frac{1}{2}\left[\left(c + \frac{1}{b}\right) \pm \sqrt{\left(c + \frac{1}{b}\right)^2 + \frac{4}{ab}}\right]$$

Here

$$a = \left[(\gamma - 1)\left(\Theta_0 - \Theta_e^{c1}(1)\right)\right]^{-1} > 0,$$

$$b = \frac{(\gamma - 1)R(1 + Z^{-1})}{1 - \eta_1} > 0$$

and

$$c = \frac{d\Theta}{d\eta}(1) < 0.$$

Note that $x_- < 0$ and $x_+ > 0$. Since $\frac{d\Theta_e}{d\eta} < 0$, we choose the negative solution above.

$$\lim_{\eta\to 1}\frac{d\Theta_e}{d\eta} = \frac{1}{2}\left[\left(c - \frac{1}{b}\right) - \sqrt{\left(c + \frac{1}{b}\right)^2 + \frac{4}{ab}}\right]$$

We now show that for $\eta < 1$ and $\eta \approx 1$, $\Theta_e > \Theta$. First note that

$$\lim_{\eta\to 1}\left(\frac{d\Theta}{d\eta} - \frac{d\Theta_e}{d\eta}\right) = \frac{1}{2}\left[\left(c - \frac{1}{b}\right) + \sqrt{\left(c - \frac{1}{b}\right)^2 + \frac{4}{b}\left(\frac{1}{a} + c\right)}\right]$$

Differentiate Eq. (15) and use Eq. (21) to show that

$$\frac{1}{a} + c = \frac{1}{Z + 1}\frac{1}{\gamma - 1}\left(1 - \frac{1}{M_0^2}\right) > 0.$$

Hence,

$$\lim_{\eta\to 1}\left(\frac{d\Theta}{d\eta} - \frac{d\Theta_e}{d\eta}\right) > 0.$$

Since $\Theta_e = \Theta$ at $\eta = 1$ and the slope of $\Theta_e(\eta)$ is more negative than the slope of $\Theta(\eta)$ near $\eta = 1$, we have $\Theta_e > \Theta$ for $\eta < 1$ and $\eta \approx 1$.

B.2 $\eta = \eta_1$

We now calculate the limit

$$\lim_{\eta\to\eta_1}\frac{d\Theta_e}{d\eta}.$$

We follow the same procedure as above to arrive at the quadratic

$$x = \frac{a}{1 + b(x - c)}$$

which has the solutions

$$x_{\pm} = \frac{(bc-1) \pm \sqrt{(1-bc)^2 + 4ab}}{2b}.$$

Here

$$a = \frac{Z(3-\gamma)+(\gamma+1)}{(\gamma^2-1)(Z+1)}\left(1 - \frac{M_c^2}{M_0^2}\right),$$

which is positive for $M_0 > M_c$. We also have

$$b = R\left(1+Z^{-1}\right)\left(\gamma^2-1\right)\frac{M_0^2}{M_0^2-1} > 0,$$

and

$$c = \frac{Z}{Z+1}\frac{3-\gamma}{\gamma^2-1}\left(1 - \frac{M_*^2}{M_0^2}\right),$$

which is positive for $M_0 > M_*$. Note that if $M_0 > M_c$, then $x_- < 0$ and $x_+ > 0$. Since $\frac{d\Theta_e}{d\eta} < 0$, we then choose the negative solution above. If $M_0 < M_c$, it can be shown that $bc - 1 < 0$, so both x_- and x_+ are negative.

C No Heat Conduction

With $\kappa_e = 0$, Eq. (10a–c) reduce to the standard Rankine-Hugoniot conditions, so that ρ and v are both constant on either side of the shock. The initial and final compression and temperature are still governed by Equation (11a), however there are no regions of continuous compression; η jumps from $\eta = 1$ in the upstream region to $\eta = \eta_1$ in the downstream region. The electron advection equation, Eq. (10d), then reduces to

$$\frac{dT_e}{dx} = \frac{\gamma_{ei}(Z+1)}{m_0 C_{v,e}}\left(T - T_e\right). \tag{30}$$

In the upstream region $T = T_0$, while $T = T_1$ in the downstream region.

Generic solutions to Equation (30) have the form

$$T_e(x) = T - Ae^{-x/L},$$

where $L = \frac{m_0 C_{v,e}}{\gamma_{ei}(Z+1)}$. In the upstream region, we require that $A = 0$ so that the solution remains bounded as $x \to -\infty$. Therefore, the upstream solution is a constant state with $T_e = T_i = T_0$. The downstream solution exhibits differential shock heating ($T_i > T_e$) and a relaxation to a constant state with $T_e = T_i = T_1$. The electron temperature, T_e, jumps from the upstream value of T_0 to the initial downstream value at the shock, which we denote $T_{e,s}$. Without loss of generality we may locate the shock at $x = 0$. We then require that $A = T_1 - T_{e,s}$ for the downstream solution.

We again use Equation (6) to derive a shock condition that determines the jump in values of T_e at the shock. In the steady frame with $\kappa_e = 0$, Equation (6) may be written as

$$\frac{dS_e}{dx} = \frac{\gamma_{ei}}{m_0 T_e}\left(T_i - T_e\right).$$

Integrating this equation over an infinitesimal domain surrounding the shock leads to the condition

$$S_{e,L} = S_{e,R};$$

for a γ–law gas, this condition becomes

$$T_{e,R} = T_{e,L}\left(\frac{\rho_R}{\rho_L}\right)^{\gamma-1}.$$

We then write $T_{e,s}$ in terms of η_1 and T_0;

$$T_{e,s} = T_0 \eta_1^{-(\gamma-1)}. \tag{31}$$

The downstream solution can then be written as

$$T_e(x) = T_1 - (T_1 - T_{e,s})\, e^{-x/L},$$

where $L = \frac{m_0 C_{v,e}}{\gamma_{ei}(Z+1)}$ and $T_{e,s} = T_0 \eta_1^{-(\gamma-1)}$. Here T_1 is given by

$$\frac{T_1}{T_0} = (1 + \gamma M_0^2)\eta_1 - \gamma M_0^2 \eta_1^2$$

and

$$\eta_1 = \frac{\gamma - 1}{\gamma + 1} + \frac{2}{\gamma + 1}\frac{1}{M_0^2}.$$

The ion temperature can be determined from Equation (12);

$$T_i = T_1 + Z(T_1 - T_{e,s})e^{-x/L}.$$